XIII Congresso Ibérico de Acústica
55º Congreso Español de Acústica
TECNIACÚSTICA 2024
Faro, 11 a 13 setembro 2024

NUMERICAL SIMULATION OF AERODYNAMIC NOISE OF HIGH-SPEED TRAINS USING A HYBRID METHOD

Ana Vieira[1], Miguel Cuadrado[1], Mario Gómez[1], Claudia Sanz[1], Jorge Cascales[1]

[1]Dirección de Innovación, Área de Acústica, Patentes Talgo SL
{anaelisa.alvesvieira@talgo.com, miguel.cuadradosierra@talgo.com, mario.gomezleal@talgo.com, claudia.sanzmoreno@talgo.com, jcascales@talgo.com}

Resumen

La expansión ferroviaria es un elemento clave para conseguir la neutralidad climática. No obstante, este crecimiento puede tener un efecto negativo en el nivel de exposición a ruido en áreas urbanas y rurales. El desarrollo de mapas estratégicos de ruido por parte de las autoridades reguladoras tiene como objetivo minimizar ese impacto, y como consecuencia, se prevé que los límites máximos de ruido permitido actuales se tornen más restrictivos. Los métodos de simulación numérica son una herramienta importante en el desarrollo de nuevos conceptos de tren. Sin embargo, la simulación numérica de un tren completo es una tarea compleja, debido a su gran dimensión. El tamaño del mallado necesario para capturar las oscilaciones del flujo de aire turbulento a alta velocidad, junto con la discretización temporal necesaria para calcular altas frecuencias, resulta en largos tiempos de cálculo, que pueden ser incompatibles con aplicaciones en la industria ferroviaria. Este trabajo presenta una metodología híbrida para el cálculo de ruido aerodinámico, basada en simulaciones de dinámica de fluidos computacional (CFD) y en el método de los elementos finitos (FEM), utilizando la analogía acústica de Lighthill. Los resultados son presentados para posiciones de observador definidas según la ISO EN 3095:2013: "Measurement of noise emitted by rail bound vehicles".

Palavras-chave: ferrovía, ruido aerodinámico, ruido de paso.

Abstract

The expansion of rail transport is considered an important step towards climate neutrality. This growth can have a negative impact on noise exposure levels in both urban and rural areas. Authorities are currently working on strategic rail noise maps to minimize this impact, and noise limits of exterior noise are expected to become stricter. Numerical simulation is a powerful tool in the decision-making process of a new train design. Simulating aerodynamic noise of a complete train, however, is a challenging task due to its dimension. The mesh refinement required to capture the turbulent flow behavior at high speed together with the short time step necessary to achieve high frequencies result in long computational times that can be unsuitable to railway applications. This work presents a hybrid approach to calculate aerodynamic noise, based on a CFD (Computational Fluid Dynamics Analysis) and a FEM (Finite Element Method) simulation of the flow-induced noise based on Lighthill's acoustic analogy. Results are presented for observer positions defined according to the ISO EN 3095:2013: "Measurement of noise emitted by rail bound vehicles".

Keywords: railway, aerodynamic noise, pass-by noise.

PACS no. 43.28.Ra, 43.20.Rz

1 Introduction

The expansion of the railway is a key factor towards an economy less dependent on fossil fuels [1]. In addition, it presents further advantages compared to other modes of transportation, such as lower operational costs and higher reliability for the passenger or cargo [2]. For these reasons, railway operations are expected to grow significantly over the coming decades [3].

A growth in the number of passenger and freight train operations, however, is expected to increase noise exposure levels in communities. Consequently, noise limits are expected to become more restrictive over the years, to protect communities and eco-systems from excessive noise levels.

Mitigation measures, such as noise barriers, night curfews and improvements in the infrastructure, can be effective but are also expensive [4]. Reducing the noise at the source is therefore the preferred solution.

Pass-by noise is composed of equipment noise, rolling and aerodynamic noise. Rolling noise is generated by the interaction between the wheels and the track, and aerodynamic noise is generated by the interaction of an unsteady flow and a solid body.

Aerodynamic noise becomes important at high speed, above 250 km/h. The pantograph and the inter-coach gap are typical sources of aerodynamic noise in a train operating at high speed.

Separating and assessing the different aerodynamic noise sources in a train is a complex task. Current literature indicates that aerodynamic noise sources in an operating train might be separated using acoustic array measurements and beamforming methods [5]. Wind tunnel measurements of scale models are also commonly used to understand the noise generation mechanisms in high-speed trains.

Establishing a ranking of the dominant noise sources during pass-by is crucial to reduce the train noise footprint. However, experimental methods are time-consuming, costly, and not always feasible due to the availability of an operating train, or access either to the track or to an aeroacoustic wind tunnel. Computational methods are therefore a more suitable approach to determine aerodynamic noise at the design phase of a new train.

In the railway industry, aeroacoustic simulations are particularly challenging due to the large dimensions of a train and the complex geometry of its components such as the pantograph or the rolling gear.

Aerodynamic noise can be calculated using different computational methods. The direct noise computation (DNC) method calculates the aerodynamic and acoustic fields simultaneously. This method has high accuracy, however, the computational resources and the time required for the calculation make it unsuitable for railway applications [6].

Hybrid methods use acoustic analogies (such as the Lighthill's or the Ffowcs-Williams Hawkings analogies) to calculate the noise source, using velocity and pressure fields determined in computational fluid dynamics (CFD) simulations. These methods are not as computationally demanding as DNC methods. On the other hand, semi-empirical methods [7] and the Stochastic Noise Generation and Radiation (SNGR) method [8] are a valid option to obtain fast estimates and to perform comparative analysis. However, these approaches are not as flexible and accurate as DNC and hybrid methods.

This research work calculates the aerodynamic noise generated in different regions of a Talgo high-speed train, using a hybrid approach that combines a Large Eddy Simulation (LES) [9] with the Lighthill's analogy [10]. These regions are the nose, first and second bogies, inter-coach gap and folded and deployed pantograph.

Section 2 describes the regions of the train considered in this work and provides an overview of the computational method. Section 3 shows the main CFD and noise results and compares a simulated pass-

by noise curve with experimental data. Finally, Section 4 summarizes the main results and conclusions of this work.

2 Methodology

2.1 Geometry simplification

A transient CFD simulation of a complete train is a challenging task, due to the fine mesh refinement and short time step required to obtain input data suitable to the aeroacoustic simulation. In this work, the train is separated in different domains, as shown in Figure 1. The domains considered in this work are the 1st and 2nd bogies, the nose, an inter-coach gap, the folded pantograph, and the deployed pantograph (not included in Figure 1).

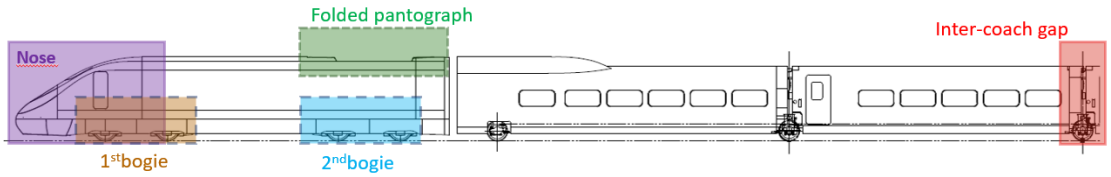

Figure 1: Separation of the train aero-acoustic sources in different domains.

The aerodynamic noise generated in each of these domains is calculated separately, which results in shorter computational times than simulating the complete train. Separating the train into different domains also allows us to identify the dominant aerodynamic noise sources during pass-by.

The geometry of the different domains was simplified to avoid overrefined meshes, without losing important geometry characteristics that might affect the turbulent air flow behaviour. Figure 2 shows the geometries of the front bogie, pantograph (folded and deployed) and inter-coach gap used in the CFD and aeroacoustic simulations.

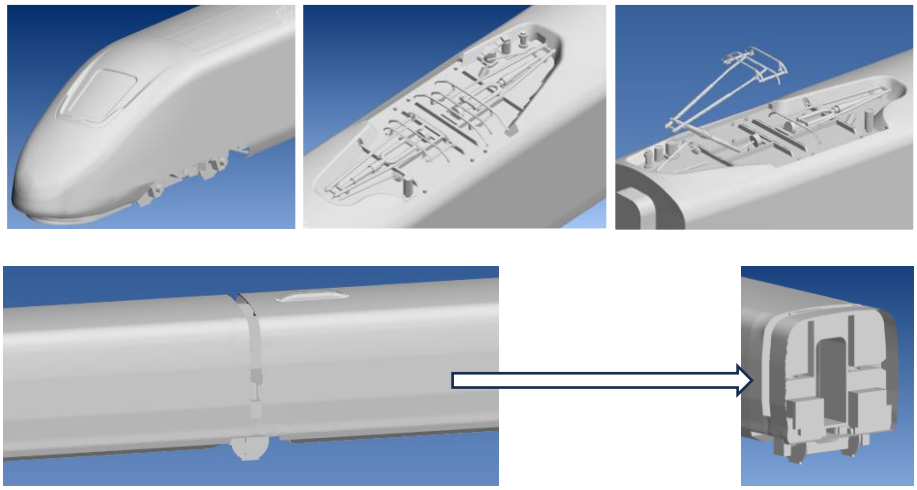

Figure 2: Geometry simplifications used in the simulation of the front bogie, folded and deployed pantograph, and inter-coach area (side view and cut in the *x*-axis section of the rolling gear).

2.2 Computational Fluid Dynamics Simulation

The CFD simulations were performed with Cradle [11], a software of Hexagon's Manufacturing Intelligence division. The meshes of the different domains were generated with the preprocessor of Cradle, using a voxel fitting approach. This method builds a voxel mesh directly from the geometry and inserts a prism-layer after the volume mesh generation.

Two different volumes are defined for each CFD simulation: a first volume to capture the flow behaviour in the region and a second volume to export the input data required to the aeroacoustic simulation. The first volume is the computational domain of the CFD simulation and should be large enough to capture a correct airflow behaviour.

Table 1 shows the dimension of the two volumes considered for each of the 6 domains calculated in this work, as well as the total number of elements.

Table 1: Characteristics of the CFD mesh generated for each domain.

Domain	CFD Volume (m) (length, width, height)	Export volume (m) (length, width, height)	Number of elements ($\times 10^6$)
Nose	75×33×14.5	7×3,5×4	51
Front bogie	130×30×14	28×6,5×2	47
Folded pantograph	134x120x61	8,5×6×7	39
2nd bogie	130×30×14	28×6,5×2	47
Inter-coach gap	65 ×33 ×11	15× 7 ×6,5	67
Deployed pantograph	134 ×120 ×61	8 ×3 ×3	17

The mesh and regions size defined in the CFD simulations vary due to the characteristics of each domain. Certain parameters, such as the size of the CFD region and the growth factor of the mesh were also optimized as this research work progressed. For example, the deployed pantograph was the last case simulated, and therefore, it was optimized based on the knowledge obtained from the previous simulations. As result, the deployed pantograph has the smallest number of elements, despite being the most complex case in terms of geometry details. As an example, Figure 3 shows a side view of the mesh used for the simulation of the inter-coach gap.

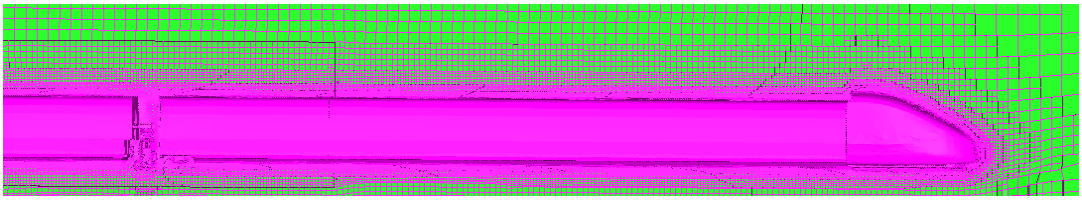

Figure 3: Side view of the CFD mesh used for the inter-coach gap.

The analyses were performed for a train velocity of 280 km/h, and therefore the airflow can be considered as incompressible. The initial conditions of the flow were obtained using a Reynolds-Averaged Navier-Stokes (RANS) model. These initial conditions were used as input in the transient analysis.

In the transient analysis, the turbulent flow was modelled using a Large Eddy Simulation (LES). The computational time varied depending on the region, between 5h (deployed pantograph) to 150h (bogies and nose). The simulations were performed in a CPU with 48 cores, 512 GB RAM and 2 processors Intel(R) Xeon(R) Gold 6248R @ 3GHz 2.99 GHz.

2.3 Aeroacoustic simulation

The aeroacoustic simulations were performed using Actran [12]. The noise sources were computed using the CFD data calculated with Cradle, through the iCFD tool of Actran. The iCFD tool reads the velocity field in the time domain, averages the data, and interpolates it to acoustic mesh in the frequency domain.

The frequency range of the acoustic analysis was limited from 200 to 1600 Hz to avoid very fine meshes. Additionally, experimental pass-by noise measurements of Talgo high speed train at 300 km/h indicate that frequencies higher than 1600Hz only contribute to increase the A-weighted equivalent continuous sound level ($L_{Aeq,T}$) in 1 dBA.

The aeroacoustic simulation aims to determine the noise generated at each region separately. Therefore, only the noise source and a small portion of the adjacent geometry are considered in the simulation. As an example, Figure 4 shows the domain considered for the front bogie. The computational domain is limited to the bogie region and the nose of the train. A first volume is used to calculate the noise source in the near-field, which is then calculated in the second volume and propagated to far-field points.

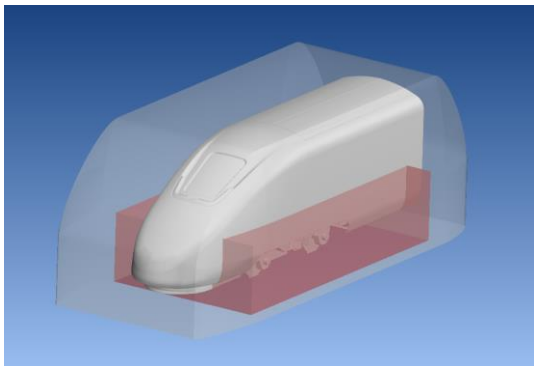

Figure 4: Volume meshes used in the aeroacoustic simulation of the front bogie.

The mesh size used in the aeroacoustic simulation was changed depending on the target frequency. Lower frequencies can be calculated with coarser meshes than high frequencies. Nevertheless, low frequencies require larger domains for the noise source computation than high frequencies. This work used different meshes for low and high frequencies, which was useful to limit the number of mesh elements, and therefore to optimize the computational time. The acoustic mesh should be coarser than the CFD mesh to ensure a valid interpolation.

The aeroacoustic field was computed using the Lighthill's analogy and the calculations were based on a FEM formulation.

The noise was propagated to the far-field using infinite elements with a non-reflective boundary. An observer position aligned with the noise source was defined at a distance of 7.5m and a height of 1.2m from the track, as defined by the ISO EN 3095: 2013 "*Measurement of noise emitted by railbound vehicles*".

The computational time varied depending on the mesh refinement considered for the different frequency ranges. The aeroacoustic simulation took approximately 1 hour per frequency step at low frequencies, and up to 5 hours per frequency step at the highest frequencies. The aeroacoustic simulation was performed in the same CPU as the CFD simulation.

3 Results

3.1 CFD results

This section presents the CFD results calculated for the six domains considered in this research work. Figure 5 shows the velocity field determined for the train nose in a *y*-axis section. The velocity increases significantly in the region of the front window, which indicates that the discontinuity between the window and the upper part of the train is the main source of aerodynamic noise in this region.

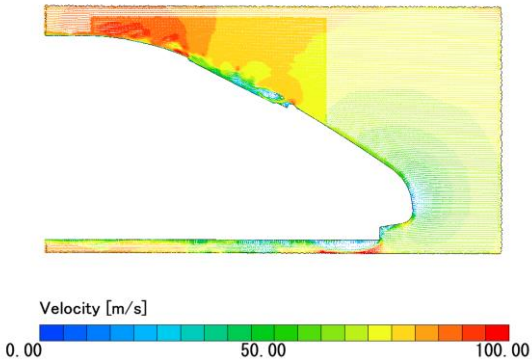

Figure 5 Velocity field calculated for the train nose.

Figure 7 shows the velocity field in the first and second bogies, which were computed together in the CFD simulation, due to their proximity, and the air flow of the front bogie affect the second bogie. The highest velocity values are observed in the first bogie.

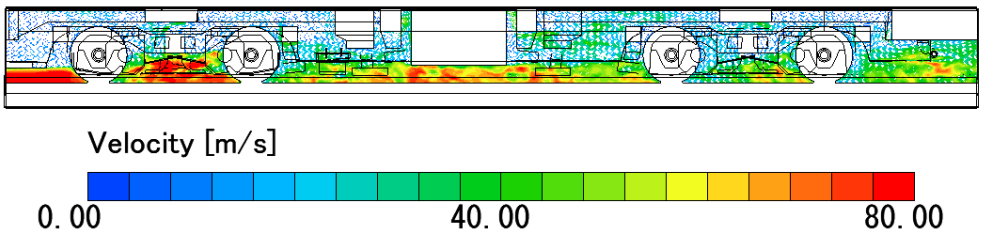

Figure 6: Velocity field in the front and second bogies.

Figure 8 displays the velocity field around the folded pantograph. The maximum values are located before and after the pantograph area, due to the discontinuity of the train surface.

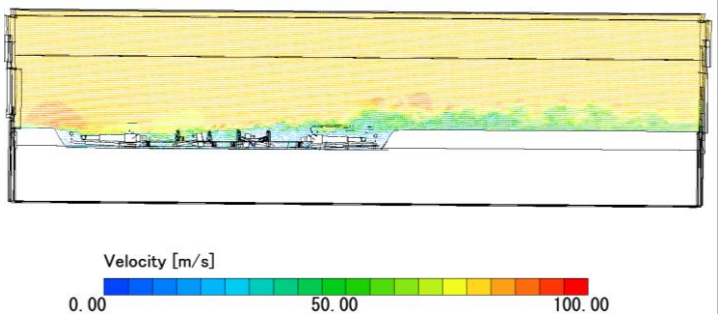

Figure 7: Velocity field in the folded pantograph.

Figure 9 shows the airflow behaviour around the deployed pantograph. There are several regions with maximum velocity values, and the airflow is visibly more disturbed than in the case of the folded pantograph.

Last, Figure 10 shows the airflow in the inter-coach gap area. The velocity values are low when compared to any of the other regions analysed in this work. The maximum values of velocity are observed in the bottom part of the inter-coach gap.

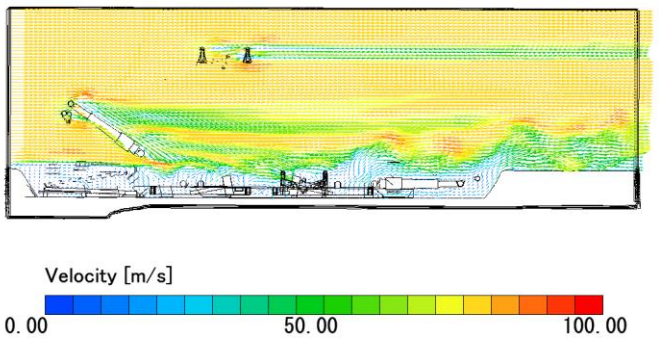

Figure 8: Velocity fiend in the deployed pantograph.

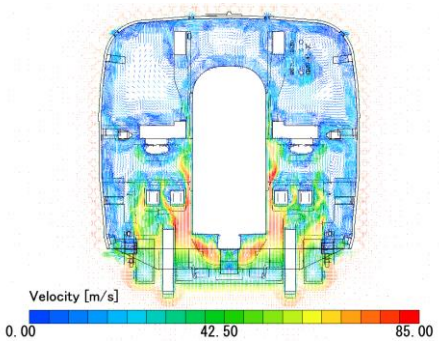

Figure 9: Velocity field in the inter-coach gap.

3.2 Aerodynamic noise results

This section presents some of the noise contour plots calculated for each domain. These plots provide important information regarding the location of the main noise source in each domain, per frequency. The plots presented in this section do include the colour scale for confidentiality reasons. The results are focused on the frequency of 400Hz, as it is one of the frequencies with the highest noise values, and the noise contours are very clear.

Figure 10 and 12 show the noise contours in the nose and bogie regions, respectively. In the nose, as expected, the higher values of noise are located close to the front window. In the 1st bogie, the maximum noise values are located between the wheels.

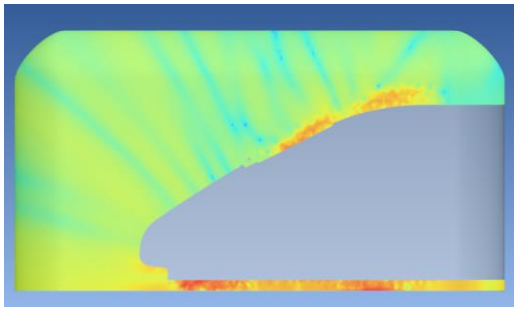

Figure 10: Noise contour in the nose (400Hz).

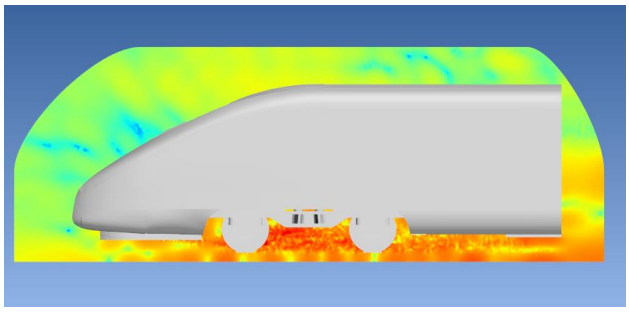

Figure 11: Noise contour in the front bogie (400Hz).

Figures 13 and 14 show the noise contours in the 2nd bogie and in the folded pantograph, at 400 Hz. The noise contour of the 2nd bogie is similar to the front bogie. The folded pantograph shows the highest noise values around the cavity. A similar behaviour is observed in the deployed pantograph (see Figure 14).

In the inter-coach gap, the noise is mainly produced in the bottom part, around the wheels, and therefore, the cavity of the inter-coach gap itself is not the main noise source.

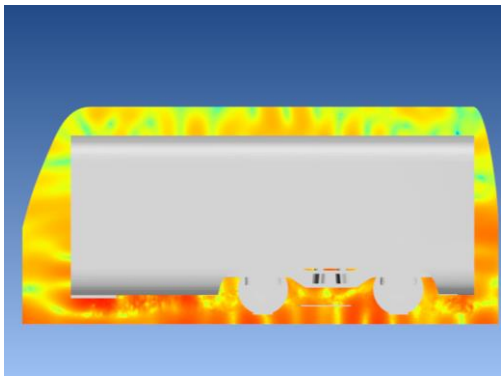

Figure 12: Noise contour in the 2nd bogie (400Hz).

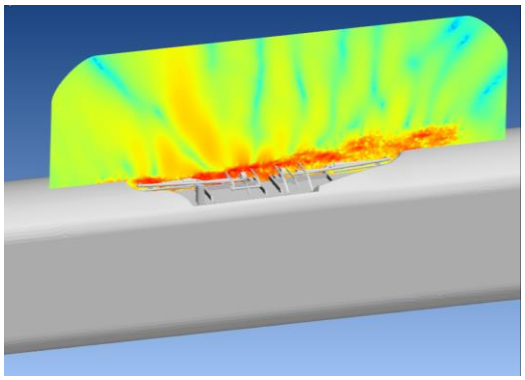

Figure 13: Noise contour in the folded pantograph (400Hz).

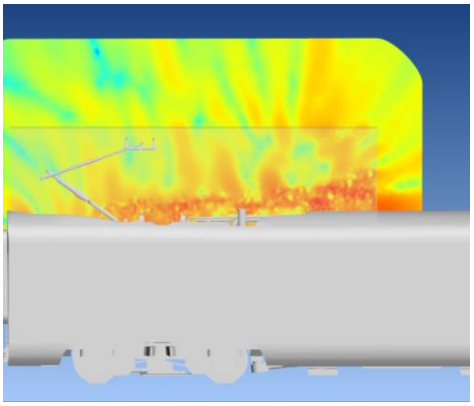

Figure 14: Noise contour in the deployed pantograph (400Hz).

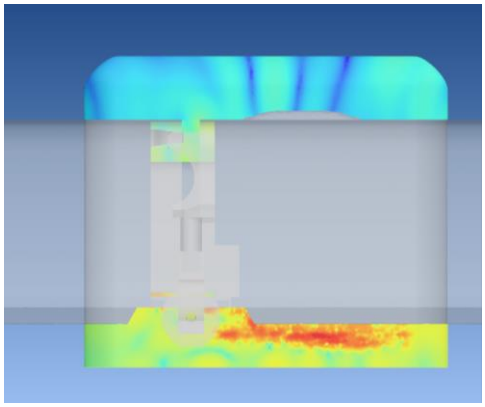

Figure 15: Noise contour in the inter-coach gap (400Hz).

3.3 Ranking of aerodynamic noise sources

This section presents a ranking of the aerodynamic noise sources present in the train at the velocity of 280 km/h. The overall sound pressure level (OASPL), in the frequency range from 200 to 1600Hz, was determined at an observer point at a distance of 7.5*m* and at a height of 1.2*m* from the track, as specified in the ISO EN 3095:2013: "*Measurement of noise emitted by rail bound vehicles*".

Table 2 shows the ranking of aerodynamic noise sources, with the results normalized for confidentiality reasons.

The noise source with the highest OASPL value at the observer position is the front bogie. This value is taken as the reference value, and the values presented for the other sources are relative to the front bogie. This means that, for example, the OASPL value found for the nose is 1dBA lower than the OASPL value calculated for the front bogie.

Based on this ranking, the front bogie, the nose, and the 2nd bogie have a similar contribution to pass-by noise. The pantograph and the inter-coach gap present a significantly lower value of OASPL than the front bogie.

Table 2: Ranking of the aerodynamic noise sources in the train at the velocity of 280 km/h (normalized). The variable *d* stands for the distance from the track, and *h* to the height relative to the top of the rail.

Domain	OASPL d=7.5m, h=1.2m
Front bogie	0 dBA (maximum value as reference)
Nose	-1 dBA
2nd bogie	-2 dBA
Folded pantograph	-8 dBA
Inter-coach gap	-8 dBA
Deployed pantograph	-10 dBA

3.4 Comparison with experimental results

This section compares the computational results with experimental data. Separating the aerodynamic noise sources from the rolling noise and from the noise produced by the different equipment such as compressors, fans and traction systems is not a simple task. Current literature indicates that beamforming methods [13] show good results in separating different noise sources, however, those methods imply a complex experimental setup and instrumentation on track.

Therefore, for the validation, the aerodynamic noise sources determined computationally were summed up to the rolling noise measured in positions close to the wheels where rolling noise is dominant. The acoustic power of the onboard equipment was added based on data provided by the suppliers.

Figure 16 compares the calculated pass-noise curve with two different measurements. The simulation presents a good agreement with the experimental data. The value of $L_{Aeq,T}$ of the calculated and an average of the two experimental curves differs in 1 dBA.

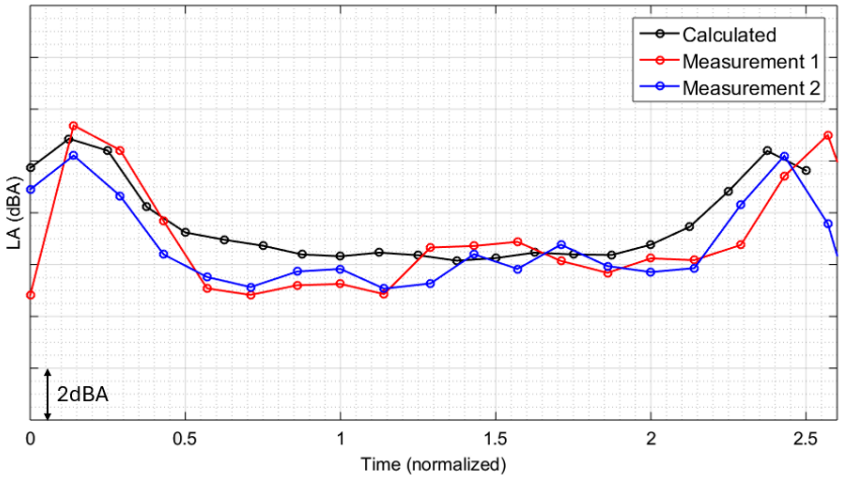

Figure 16: Calculated pass-by noise curve (normalized) compared to two different measurements (velocity of 280 km/h).

The head and the tail present a good fit with the experimental data, showing that the values determined for the pantograph (folded and deployed) are realistic. Many literature sources refer that the pantograph is a dominant noise source [14], however, that is not observed in Talgo high-speed trains.

Figure 17 shows the different components considered in the calculation of the pass-by noise curve. Equipment noise, at the speed of 280 km/h, can be neglected, as it is not relevant to the overall noise. In the middle region of the train, the rolling and aerodynamic noise seem to have the same contribution at this velocity, which is in line with current literature. Aerodynamic noise sources are particularly important in the beginning of the curve, a region that corresponds to the 1st and 2nd bogies, nose, and folded pantograph.

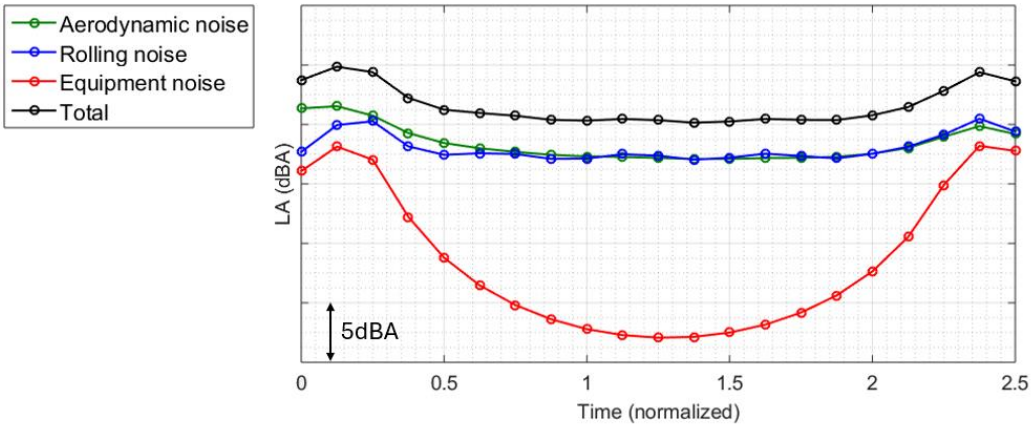

Figure 17: Different noise components during a pass-by at 280 km/h.

4 Conclusions

This work determined the aerodynamic noise generated by different regions of a high-speed train at the operating velocity of 280 km/h. The aerodynamic noise contribution of the 1st and 2nd bogies, nose, folded and deployed pantograph and inter-coach gap was calculated using a hybrid approach.

The velocity field in each region was determined with a LES. This data was used as input in an aeroacoustic simulation based on the Lighthill's analogy. The near-field results were propagated to the far-field using infinite elements.

The velocity and noise contour plots are presented for different regions of the train, which allows to identify problematic areas, with higher values of aerodynamic noise. In addition, a ranking of the aerodynamic noise sources originated during a pass-by at high speed was presented. It was found that the dominant noise source is the front bogie, closely followed by train nose and the 2nd bogie and.

Experimental values of rolling noise and equipment noise were added to the calculated aerodynamic noise and propagated to the far-field. The resultant pass-by noise curve was compared to experimental data. The calculated and experimental pass-by noise curves (considering frequencies from 200 to 1600Hz) show a good agreement, with a 1 dBA difference in $L_{Aeq,T}$.

Future work will focus on improving the calculation time in order to reach higher frequencies, beyond the maximum frequency of 1600 Hz considered in this work.

References

[1] D. d. F. Soares, S. Eliziario and J. D. Galvincio, "Greenhouse Gas Emissions in Railways: Systematic Review of Research Progress," Buildings, vol. 14, no. 2, 2024.

[2] R. Barcikowska and E. Wawrzyn, "Selected Sources of Research Funding in Railway Transport," WUT Journal of Transportation Engineering, vol. 136, pp. 85-99, 2023.

[3] M. Nold and F. Corman, "How Will the Railway Look Like in 2050? A Survey of Experts on Technologies, Challenges and Opportunities for the Railway System," IEEE Open Journal of Intelligent Transportation Systems, vol. 5, pp. 85-102, 2024.

[4] R. Pieren, F. Georgiou, G. Squicciarini and D. Thompson, "Auralisation of combined mitigation measures in railway pass-by noise," in InterNoise, Glasgow, UK, 2022.

[5] J. Zhang, G. Squicciarini and D. J. Thompson, "Implications of the directivity of railway noise sources for their quantification using conventional beamforming," Journal of Sound and Vibration, vol. 459, no. 27, 2019.

[6] J. Friedrich and M. Schafer, "Acoustics Simulation in the Presence of Moving Interfaces in Multiphase Flows," in 6th European Conference on Computational Mechanics, Glasgow, 2018.

[7] J. Solé and P. Huguenet, "Good practices in railway vibration prediction using empirical and hybrid models," Procedia Engineering, vol. 199, pp. 2669-2674, 2017.

[8] B. d. Brye, A. Poulos, C. Legendre and G. Lielens, "A cost-effective computational technique for aeroacoustic," in ISMA 2020 Conference, 2020.

[9] J. Ferziger, "Large Eddy Simulation: An Introduction and Perspective," in New Tools in Turbulence Modelling. Centre de Physique des Houches, Berlin, 1997.

[10] S. Caro, P. Ploumhans and X. Gallez, "Implementation of Lighthill's Acoustic Analogy in a Finite/Infinite Elements Framework," in 10th AIAA/CEAS Aeroacoustics Conference, Belgium, 2004.

[11] HEXAGON, "Cradle CFD Version 2021 Release Notes," 2021.

[12] HEXAGON, "Actran 2022 - User's Guide ActranVI," 2022.

[13] I. L. Arteaga, M. Rissmann, M. Á. Garralaga, D. Thompson, M. Abom, E. Cierco, M. Dittrich, E. Sarradj and M. Garcia, "The TRANSIT project: innovation towards train pass-by noise source characterisation and separation tools," Transportation Research Procedia, vol. 72, pp. 989-996, 2023.

[14] M. Ikeda, T. Mitsumoji, T. Sueki and T. Takaishi, "Aerodynamic Noise Reduction of a Pantograph by Shape-Smoothing of Panhead and Its Support and by the Surface Covering with Porous Material," Noise and Vibration Mitigation for Rail Transportation Systems. Notes on Numerical Fluid Mechanics and Multidisciplinary Design, vol. 118, p. 419–426, 2012.

[15] T. Tonai, E. L. Iglesias, T. Uda, T. Kitagawa, J. M. Paniagua and J. G. García, "Component-Based Model to Predict Aerodynamic Noise from High-Speed Train Bogies," Noise and Vibration Mitigation for Rail Transportation Systems, pp. 199-208, 2024.